CHAPTER V

POWER-SUPPLY SYSTEMS AND TEST SOLAR CELLS

By John L. Patterson
Langley Research Center

SECTION I - INTRODUCTION

Conversion of solar energy with photovoltaic solar cells was decided to be the most practical means of meeting the low-level power requirements throughout the desired 1-year lifetime of the satellite. Rechargeable batteries were necessary to supply all power required during the orbital dark periods, as well as to supply a large part of the power required during interrogations in sunlight.

Two separate solar power supplies were installed, one for each telemeter. Each supply was required to furnish 10 milliamperes of standby current and 110 milliamperes during interrogations at 12 volts nominal. The power supplies were designed for 1-minute interrogations during each orbit; orbital periods were approximately 100 minutes and orbital dark times varied from 0 to 35 percent of each orbital period. In addition, the satellite was to be spin stabilized at 200 rpm at launch, but was expected to tumble at approximately 20 rpm after several weeks.

In addition to the solar cells used for power, five groups of solar cells were mounted on the forward shell to obtain data on the relative effectiveness of protective covers for the cells.

SECTION II - POWER-SUPPLY SOLAR CELLS

General.- The mounting arrangement of the solar cells on the forward shell is shown in figures V-1 and IV-33. Since the payload was not separated from the final rocket motor, and because of the limited diameter of the heat shield, it was not practical to have cells facing aft. For each of the two power supplies, one tray was located on the forward end of the forward shell and four were equally spaced around the cylindrical surface. This was equivalent to having cells on five sides of a cube for each power supply. The smaller trays are solar-cell test groups and are not connected to the power supplies; these are described later.

Figure V-2 is a photograph of a typical solar-cell tray, and figure V-3 is a drawing of a tray mounted on the aluminum heat-transfer band. A rather stiff tray with flexible mounting brackets was considered necessary because the forward shell (especially in its early design) could possibly experience high-amplitude vibrational deflections during the launch operations. Forty solar cells, in eight 5-cell "shingles," were cemented to the 1/8-inch-thick

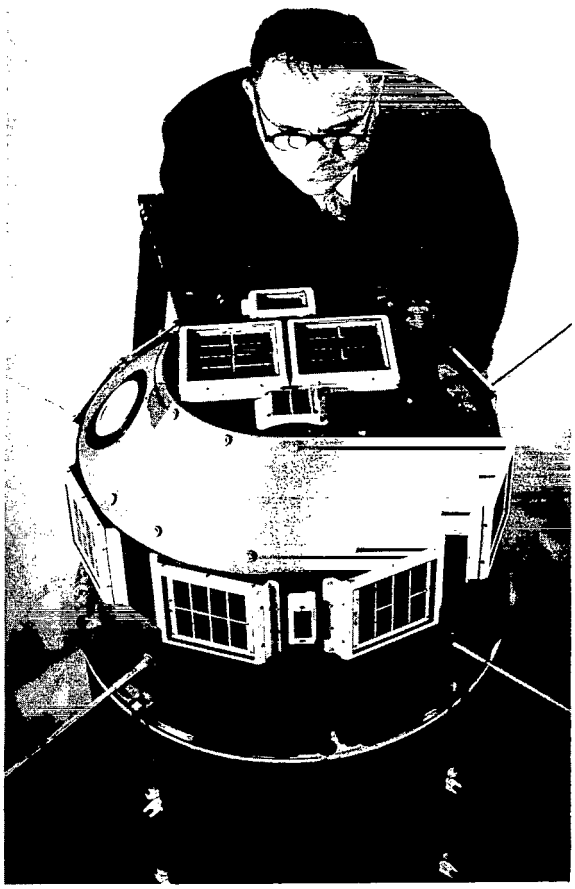

L-61-2146
Figure V-1.- Nose shell of Explorer XIII showing solar-cell trays.

magnesium alloy base of the tray. The magnesium alloy was chemically treated to provide for the electrical insulation of the cells and to improve the cement bond.

For thermal-balance requirements, the external metal surfaces were coated with an aluminum oxide coating. For good heat transfer between the trays and the aluminum band, the surfaces in contact were left bare, and those closely spaced were coated with flat black paint. Since the transmission of the fused quartz windows is low for infrared radiation, most of the excess energy absorbed by the solar cells had to be conducted out through the base to be radiated by other external surfaces. Hence, coatings or glass covers designed to improve the emissivity of the cells were not used, and low absorptivity was specified for the other exposed surfaces under the windows.

Cements.- A number of materials were investigated to find one suitable for cementing the solar cells to the trays and for coating the exposed surfaces between and around the cells. The cement had to provide good thermal conduction, and had to be flexible enough to isolate the fragile cells from mechanically and thermally induced stresses. The latter was critical since the thermal coefficient of expansion of silicon is 2.5×10^{-6} in./in./°C compared with 25×10^{-6} in./in./°C for the magnesium alloy, and the preliminary estimate of the expected solar-cell-temperature range was from -65° C to +135° C. The cement also had to withstand the space environment; tests were made to determine relative flexibility, immunity to a vacuum, and resistance to ultraviolet and ionized-particle radiation.

Silicone rubber cements were among those investigated. The one selected is a white, room-temperature-cured silicone rubber that remains flexible down to approximately -70° C. Its adhesive properties were excellent for this application when the surfaces were primed as recommended. It was found to have a solar absorptivity of 0.32, and its properties were unaffected when subjected to ultraviolet radiation at elevated temperatures. Its thermal conductivity of 7.44×10^{-4} gm cal-cm/cm^2/sec/°C compares favorably with other cements. No trouble was experienced with entrapped gas, and its rate of weight loss in a high vacuum was found to be relatively low. This cement was subjected to

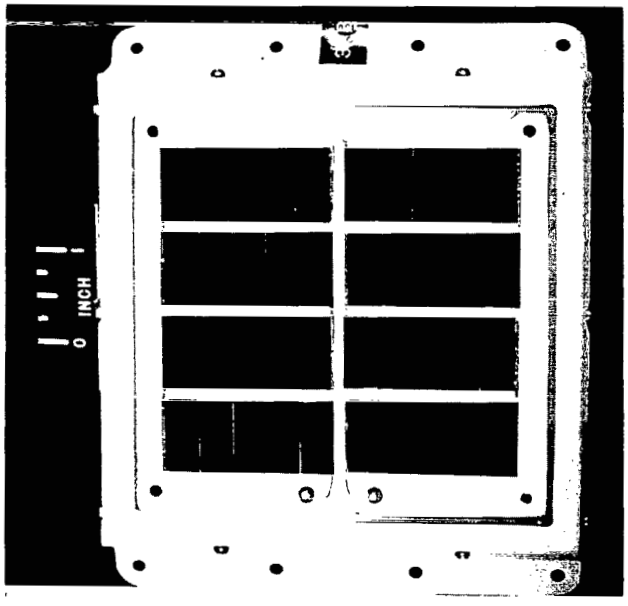

L-60-8387

Figure V-2.- Photograph of power solar-cell tray.

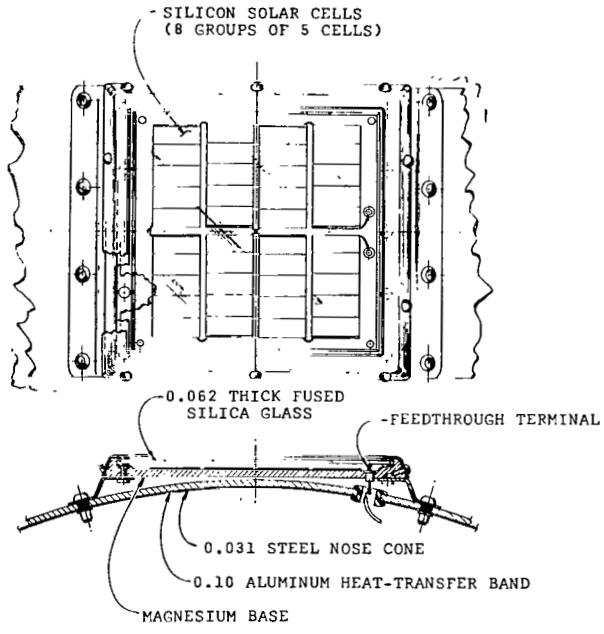

Figure V-3.- Drawing of power solar-cell tray.

proton irradiation in several cyclotrons in conjunction with solar-cell testing, and negligible damage was found.

Windows.- Fused quartz windows 1/16 inch thick (fig. V-3) were used to help protect the solar cells from possible damage by ionized particle radiation and micrometeorites. A molded silicone rubber gasket was used to cushion the windows from the stresses of launch vibrations and temperature changes. The gaskets suffered only minor surface hardening when subjected to ultraviolet irradiation at elevated temperatures.

The fused quartz was found to transmit 93 percent of normally incident light in the spectral range of the solar cells. Thoroughly sandblasting the exterior surface with fine alumina to approximate the possible effects of micrometeorite erosion was found to reduce the 93-percent transmission to 89 percent. Proton irradiation tests (ref. V-1) showed that the quartz should not be appreciably darkened by particle radiation in the expected orbit. (The artificial electron belt did not exist at this time.)

Solar-Cell Characteristics.- The nongridded silicon solar cells used for the power supplies were 1 by 2 centimeters in size, and were the P on N junction type. They were supplied in five-cell shingles without coatings or glass covers. The nominal efficiency of the cells varied from 8 to 9 percent. This efficiency rating was based on the maximum power output at 27° C when illuminated by the sun under standardized conditions on the surface of the earth (one air mass or m = 1). The actual efficiency in space at 27° C was estimated to be 0.83 of the nominal value because a large part of the increased solar energy available above the atmosphere (140 mw/cm^2) falls outside of the spectral range of the solar cells (refs. V-2 and V-3).

Tungsten filament lamps, with their voltages adjusted to give filament temperatures of 2,900 ± 100° K were used with a 1-inch-thick water filter when determining the output of the solar cells. The light intensity was monitored with a "standard" solar cell which was calibrated under standardized conditions in sunlight (m = 1), and in light from tungsten lamps when using the same type of filter and range of filament temperatures.

The curves of current output plotted against voltage at various temperatures for a typical solar-cell tray of 40 series-connected cells is shown in figure V-4. The points of maximum power output are indicated. In these tests the light intensity was adjusted to be equivalent to one solar constant ($140 \times 0.83 = 116$ mw/cm^2 as measured with a calibrated standard solar cell). It will be noted that the cells are essentially constant current generators up to a voltage that is dependent on temperature. The operating voltage is fixed by the load, and in this power supply, is primarily fixed by the batteries. A typical value of 14.8 volts (0.37 volt/cell) is indicated in figure V-4. The effect of temperature on output, when charging batteries at a nearly constant voltage, is further illustrated in figure V-5 where the data of figure V-4 are plotted as current and power output, at 14.8 volts, as a function of temperature. Since literature on solar cells often gives the change in maximum power with temperature, the measured values of this parameter are shown for comparison.

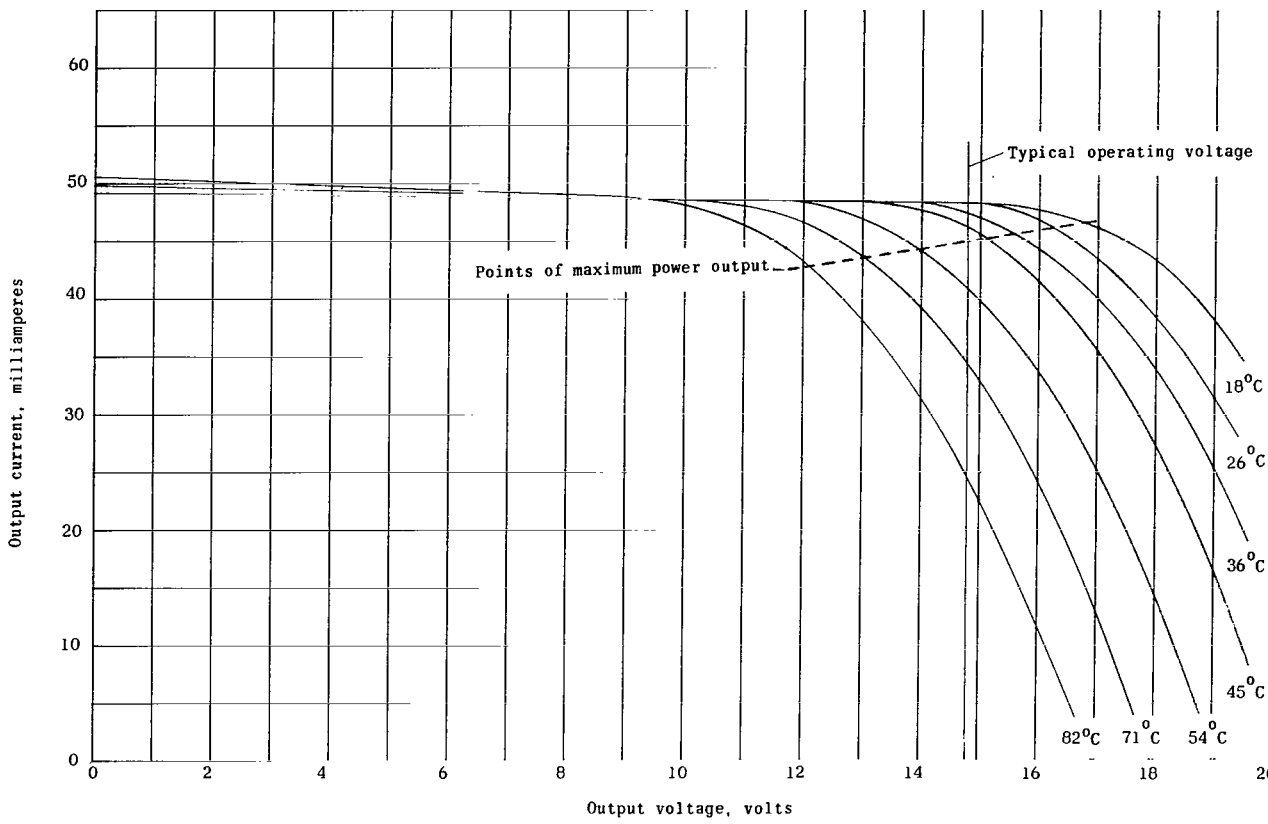

Figure V-4.- Variation of output current with voltage and temperature of a typical power solar-cell tray.

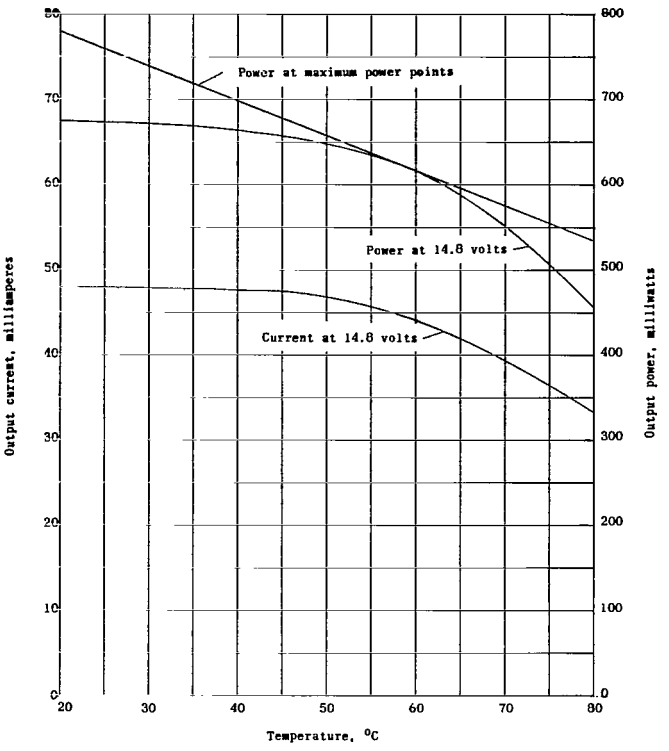

Figure V-5.- Variation of output current and power with temperature of a typical power solar-cell tray.

Effect of Vehicle Attitude.- The effect of the vehicle attitude on the output of the solar cells with respect to the sun was important because the vehicle had no cells facing aft, and was expected to remain spin stabilized only a short time. Also, the information was required to avoid an initial spin-stabilized attitude with insufficient solar-cell illumination. The output of a solar cell is approximately proportional to the projected illuminated area and hence to the cosine of the angle of the incident light. Measured values of the percent reduction of output current are plotted against incidence angle in figure V-6 with a cosine curve shown for comparison. Currents were measured under simulated battery charging conditions using a five-cell shingle. A quartz window was mounted over the cells during the test, but the effects of the tray-edge shadows were not simulated. Also shown in figure V-6 is a curve obtained in a similar manner with the sandblasted window (mentioned previously) mounted over the cells. This curve illustrates the possible effects of micrometeorite erosion, but the data were not used in the following computations.

Figure V-7 gives the predicted combined percentage of output of the solar cells of one power supply plotted against sun incidence angle computed from the experimentally determined values of figure V-6. In this case, it was assumed that the vehicle was in a pure tumbling mode (no roll), and that the rays of the sun, the vehicle roll axis, and the normal to the three trays involved were in the same plane (see sketch in fig. V-7). The ordinate is the relative output referred to one tray illuminated at normal incidence, and hence is the percentage to be applied to the output values given in figures V-4 and V-5. The computation merely required the graphical or numerical summation of the instantaneous output of each illuminated tray. The relative output is also shown as computed from the ideal cosine curve. Since the average value of a half-wave rectified sinusoidal wave is $1/\pi$, the ideal average output, over one cycle of tumbling, of the three trays is $3/\pi$ times, or 95.5 percent of that of one tray illuminated at normal incidence. This compares with a value of 87 percent found from the area under the curve of figure V-7 obtained from measured values. It can be shown that this should be very close to the minimum output averaged over any complete cycle of tumbling.

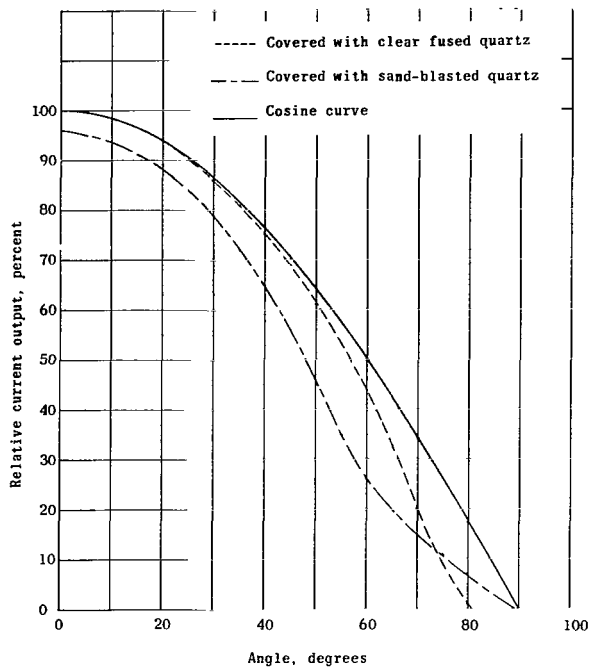

Figure V-6.- Variation of solar-cell output current with angle of incident light.

If the vehicle is assumed to be spin stabilized with the sun vector normal to the vehicle axis, four trays are illuminated in sequence, and the ideal average output is $4/\pi$ times (127 percent) that of one tray. By using measured values, the corresponding average was found to be 116 percent of one tray. In the more general case where the vehicle is spinning but the sun is not normal to the axis, the computation is more involved. When the sun is forward of the vehicle equator, a maximum of three trays can be illuminated at one time. When the vehicle is in a pure spinning mode, the tray on the forward end has a constant ideal fractional output of $\cos \phi$. From spherical trigonometry, the cosine of the angle between the sun vector and the normal to a reference tray on the cylindrical surface is $\sin \phi \cos \theta$, where ϕ is the angle between the sun vector and the vehicle axis, and θ is the angle in roll measured from the normal of the reference tray. (Refer to the sketch in fig. V-8.) The cosine of the corresponding incident angle of the illuminated tray adjacent to the reference tray is $\sin \phi \cos(90 - \theta)$ or $\sin \phi \sin \theta$. Hence, the combined fractional ideal output of the three illuminated trays is:

$$\cos \phi + \sin \phi \cos \theta + \sin \phi \sin \theta$$

The average of this expression over a period of roll is:

$$\cos \phi + \frac{4}{\pi} \sin \phi$$

When the angle ϕ (fig. V-8) is greater than 90°, the solar-cell tray on the forward end is not illuminated, and the first term in each of these expressions becomes zero. The ideal average output while spinning, computed from the second expression for values of ϕ from 0° to 180°, is shown as the dotted curve of figure V-8. The solid curve gives the corresponding predicted values based on the experimental results of figure V-6 (with clear quartz). These were computed, at each 10° increment of ϕ, by substituting measured values for each of the terms in the first of the above expressions to get variation in the combined output over 90° of roll. The averages were then obtained with the trapezoidal rule.

When all the components of a power supply were available, a completed forward shell was rotated by a motor to various angles of ϕ while illuminated by

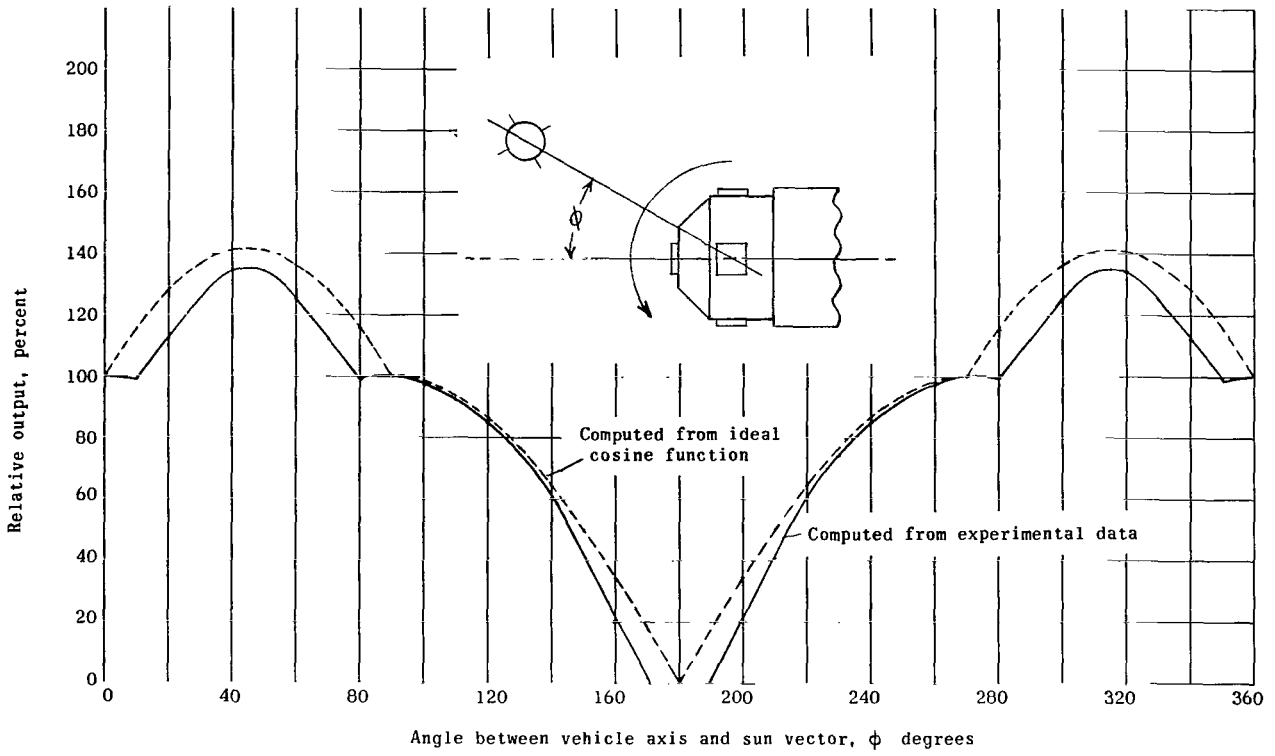

Figure V-7.- Output of solar cells in tumbling mode giving least average output.

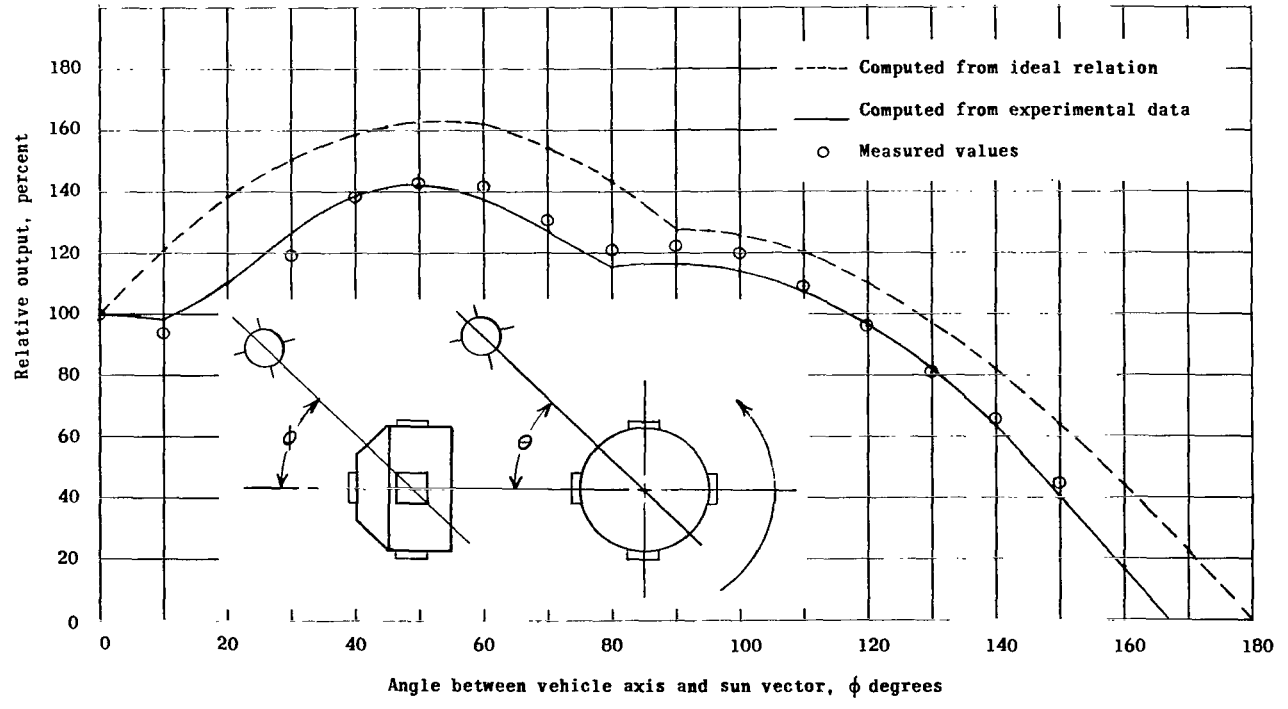

Figure V-8.- Average output of solar cells with vehicle spin stabilized at various angles between vehicle axis and sun vector.

the sun on a clear day. With the five trays properly connected in the power-supply circuit, the combined solar-cell current was plotted against angle of rotation on an X-Y plotter. Figure V-9 is an example of the curves obtained. It was plotted at $\phi = 110^{\circ}$, and the ragged dips occurred as the antenna shadows passed over the cells. The average values obtained from the areas under these curves are presented as the circled data points in figure V-8. Since it was not practical to eliminate all reflected sunlight, particularly when ϕ was close to 90°, some of the values are too high. All of the circled data points should be below the predicted curve because shadows from the tray edge and the antennas were not considered in the prediction. Antenna shadows appeared on the trays between ϕ of 105° and 135°, and their effect on the average output is noticeable but not excessive. This effect is due, in part, to the fact that at the time antenna shadows fall on a tray, another tray is illuminated and is therefore free of shadows. Figure V-8 indicates that while the vehicle is spin stabilized, an output almost equal to or greater than that of one tray normally illuminated is predicted for ϕ from 0° to 120°. This range approximately determines the limits on the angle between the vehicle axis and the sun vector at orbital injection.

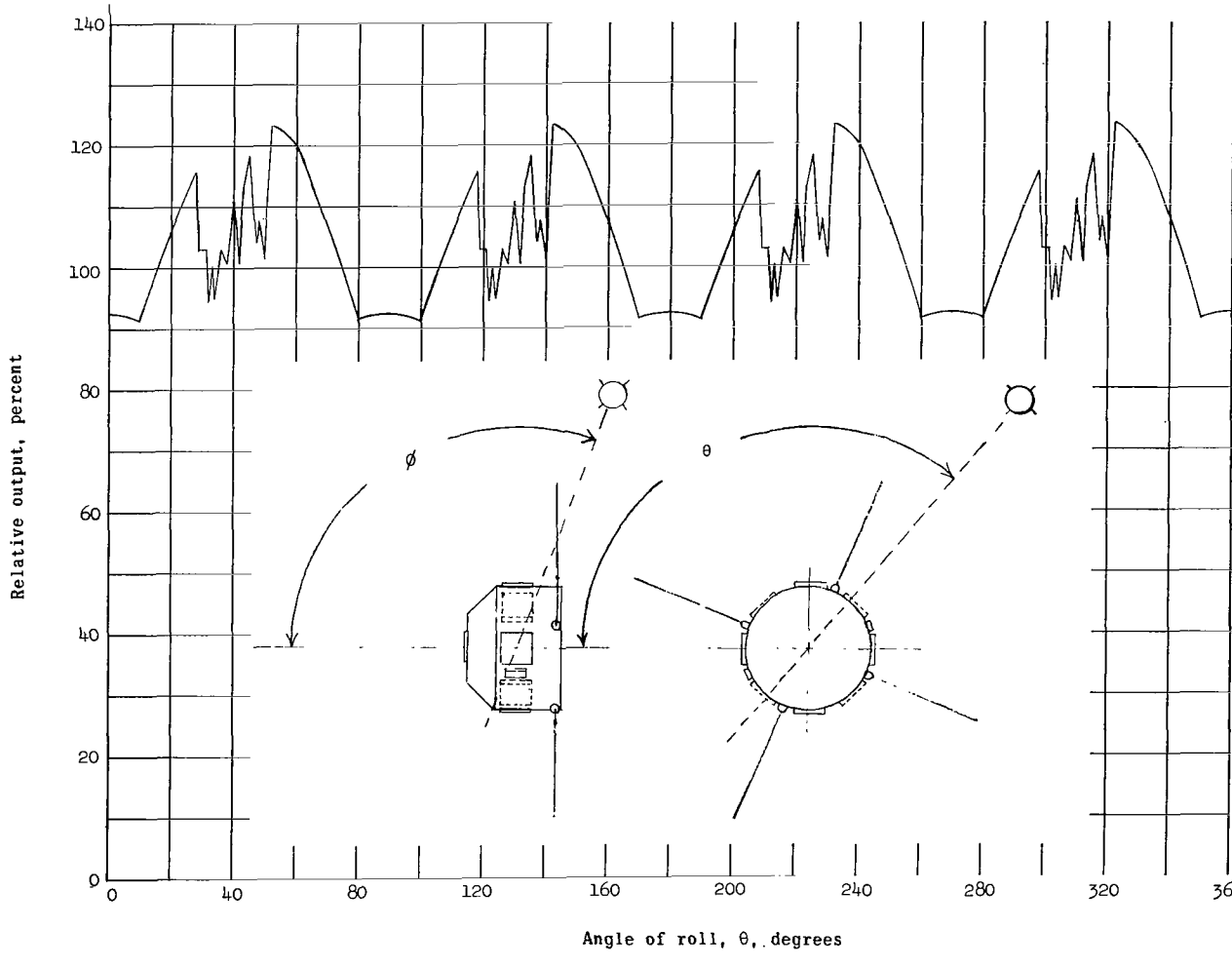

Figure V-9.- Output of solar cells with vehicle spin stabilized at $\phi = 110^{\circ}$.

The output of the solar cells after tumbling begins is difficult to predict. After all roll motions have ceased, the average output during tumbling could vary from the minimum of 87 percent as illustrated by figure V-7 to a maximum of about 136 percent. This maximum would occur when the sun vector is normal to the vehicle roll axis and midway between two trays. In general, the average output during tumbling (in each period of orbital sunlight) should approach the long-term average computed for random orientation to the sun, particularly when there is still some roll coupled with the tumbling motions. If a single solar cell or single tray of solar cells is randomly oriented to the sun, it can be shown (appendix A) that its long-term ideal average output will be one-fourth of its output at normal incidence. Hence, the five trays in each power supply were expected to have a combined ideal average percentage output of 125 during random tumbling. By using weighting factors proportional to the incremental solid angles involved (appendix B), the solid curve of figure V-8 was numerically integrated to obtain a value of 105 percent with respect to one tray at normal incidence for the output during random tumbling based on measured values. This was rounded off to 100 percent for estimation purposes.

The output of the power solar-cell trays due to reflected light from the earth was omitted in the preceding discussion. The additional output is difficult to predict, and in general, it will be small because when batteries are being charged, the output of a tray drops rapidly at low light intensities.

Qualifying Tests.- Before the shingles were cemented to the trays, they were all given a series of tests to eliminate defective units and to determine their electrical characteristics. To check for defective intercell bonds, the shingles were mechanically loaded in bending with a 250-gram weight while resting on supports 4.4 centimeters apart. In the routine electrical tests, values of short-circuit current, open-circuit voltage, output current at 1.85 volts (0.37 volt/cell), and output voltage at 36 ma were obtained. The acceptable cells were matched to provide the most efficient operation when connected in series on a tray. Emphasis was placed on current at 1.85 volts, and on the general shape of the current-voltage curve. The cells for the various trays of each supply were also selected to have approximately the same characteristics.

The acceptable cells with the lowest output were cemented to trays for the prototype vehicle. These were subjected to the environmental tests described in chapter VII both individually and while mounted on the forward shell. Subsequent trays were only given vacuum and temperature cycling tests before installation. Environmental testing after installation was considered more realistic - particularly vibration and impact tests because of the very large amplifications experienced. Initially, and after each test, the trays were illuminated to obtain the four parameters listed in connection with the shingle tests. Finally, data were taken to obtain the curve of room-temperature current plotted against voltage for each tray.

Proton Irradiation Tests.- The quartz windows were expected to give some shielding from the electrons and low-energy protons in space, but there was concern about the effects of high-energy protons, especially since the initial estimate of apogee was 1,275 miles. (The artificial electron belt did not exist at this time.) Hence, when a program was initiated at the NASA Langley Research Center to subject electronic components to proton irradiation, various types of

solar cells were included. A number of tests were made on cells ordered for Explorer XIII. Reference 1 gives the results from the preliminary tests made with proton energies of 22 and 240 Mev. Later unreported tests were made at 40 and 440 Mev as well as additional tests at 22 and 240 Mev. The damage rate varied with proton energy, and was not the same for supposedly identical cells, but the curve in figure V-10 is thought to be a typical plot of the degradation of the output current against integrated proton flux. If for the finally predicted orbit, 500 protons/cm^2/sec be assumed for the flux of relatively high-energy protons, the curve of figure V-10 shows that the solar cells will be degraded 9 percent in 1 year.

SECTION III - BATTERIES

General.- The battery cells used were the sealed, nickel-cadmium, "button"-type cells. Their capacity rating was 500 milliampere-hours (mah) and in each power supply, 10 cells were connected in series to make a nominal 12-volt battery. A battery before potting is shown in figure V-11. The blocking diodes, described later, were also installed in the 5.5-inch-diameter, 1-inch-thick secondary battery module. To aid in sealing the cells, and to prevent working of the cases under internal pressure, the cells were potted in an unfilled epoxy resin.

A number of considerations influenced the selection of these cells for this application. A cell with a welded case closure and glass-to-metal seals around

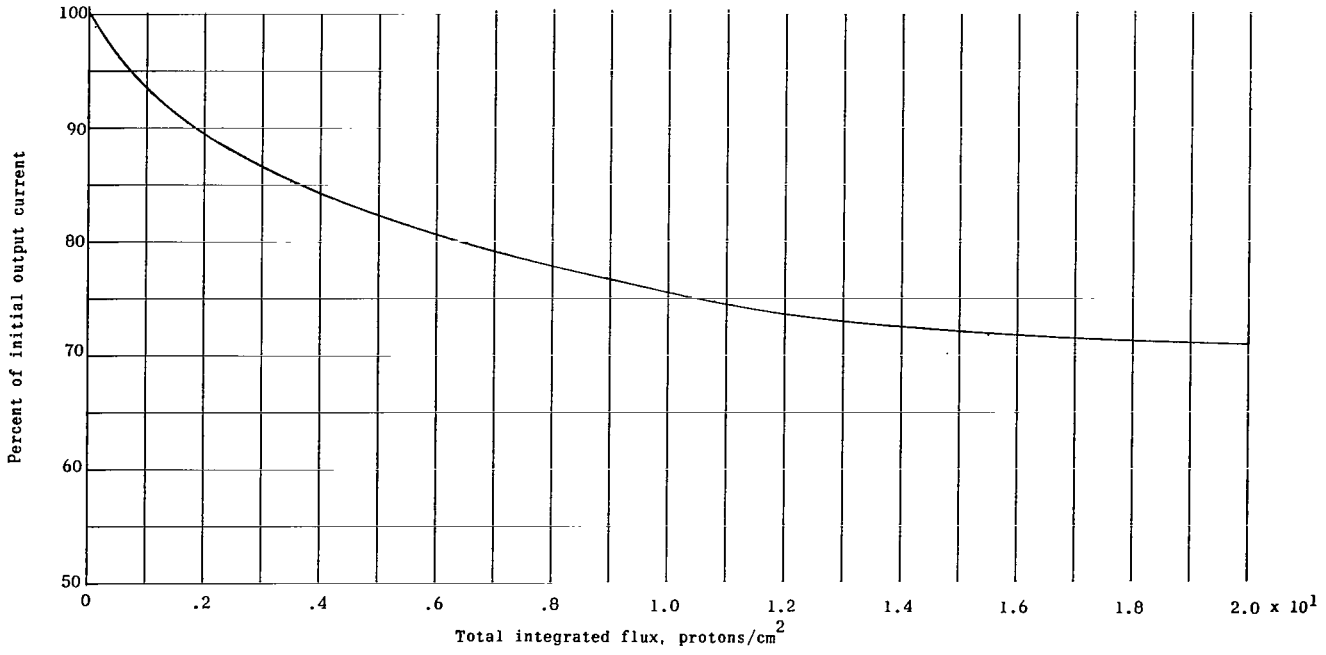

Figure V-10.- Degradation of solar-cell output-current with integrated proton flux in a 240 Mev proton beam.

the electrical leads was desired but was considered too large. Instead, it was decided to use the button cells having plastic seals, to pot them in epoxy, and to install them in the pressurized telemeter canisters. In addition, it was found that in the small cell size desired, the flat plates in the button cells were less liable to short as the separator material deteriorated than cells employing the wrapped-plate construction. For long cyclic life, it is generally recommended that the discharge per cycle be less than 10 percent of capacity. In this power supply, the maximum discharge per orbit is less than 2 percent of capacity even when interrogations are made in darkness. However, it was decided that the 115-ma load during interrogations would adversely affect the life of a cell with a capacity of much less than 500 mah. In addition, as explained later, a smaller cell would be more difficult to protect from overcharging.

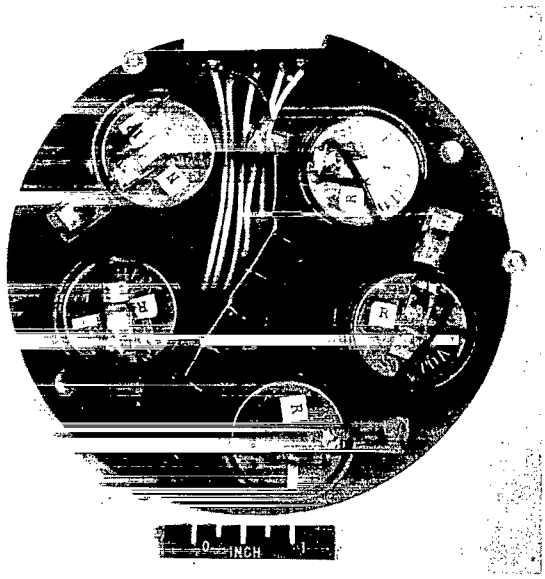

L-60-7065
Figure V-11.- Secondary nickel-cadmium battery module before potting.

Battery Cell Characteristics.- Figure V-12 gives two voltage-time curves of a typical 10-cell battery used on Explorer XIII taken at room temperature while being discharged at 100 ma. This was the discharge current at which the nominal capacity of 500 mah was rated. When obtaining the solid curve, discharge was started immediately after overcharging at 30 ma. For the dotted curve, the battery was initially being overcharged but was discharged at 10 ma for 35 minutes (maximum expected orbital darkness) before start of the 100-ma discharge. These voltages vary with temperature and discharge rate and, as illustrated, are considerably influenced by prior operating conditions. The upper curve of figure V-13 gives the discharge voltage plotted against the temperature of a typical battery when interrogations in orbital sunlight were simulated. The readings were taken near the end of the 1-minute interrogation, and the battery was supplying about 75 ma (the solar cells supplied the rest of the load). The lower curve gives the voltages obtained with conditions the same except interrogations in darkness were simulated. The battery was supplying the entire 110-ma load, and before interrogation, had been supplying the 10-ma standby load. In each case, readings were taken after 10 or more cycles (simulated orbits) to allow time for the cyclic voltages to settle down.

For long life, the charging voltage of sealed nickel-cadmium cells should be limited to prevent irreversible formation of hydrogen gas. The maximum safe value is thought to be from 1.45 to 1.50 volts per cell, and to allow for cell differences, a value of 14.2 volts was used for the 10-cell batteries. The curves of figure V-14 relate charging voltage, charging current, and temperature at two typical charging conditions. The data for the solid curves were

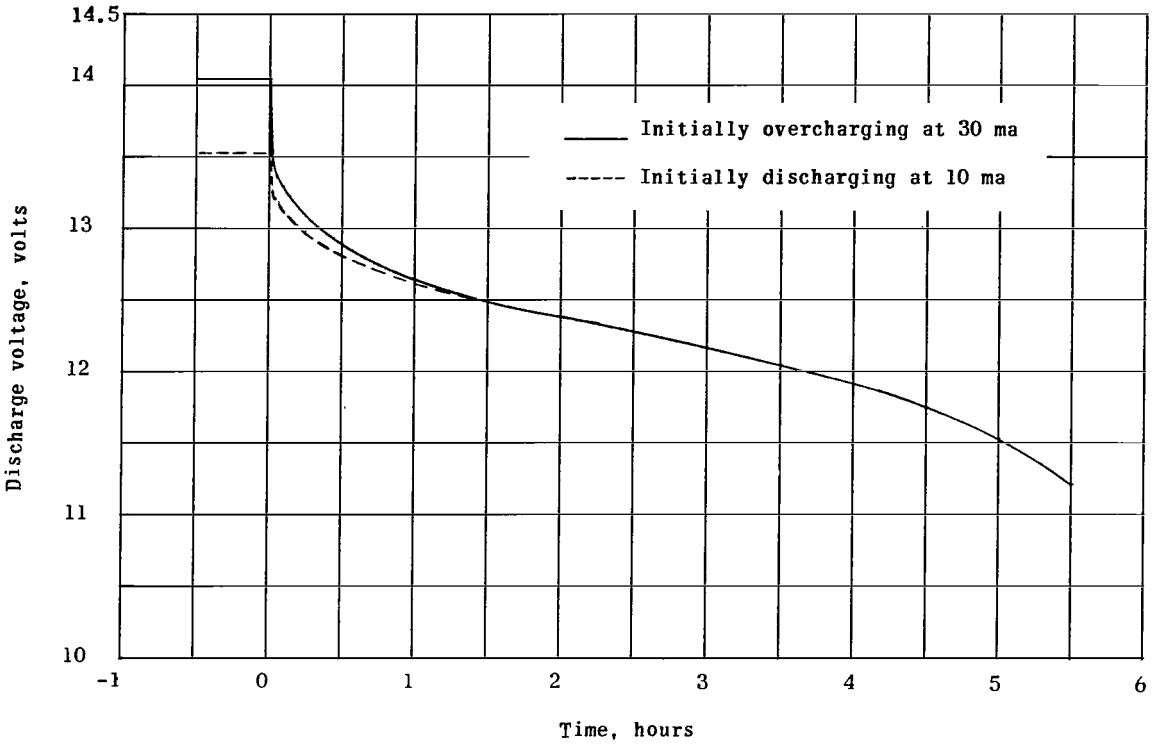

Figure V-12.- Variation of battery voltage at discharge current of 100 ma.

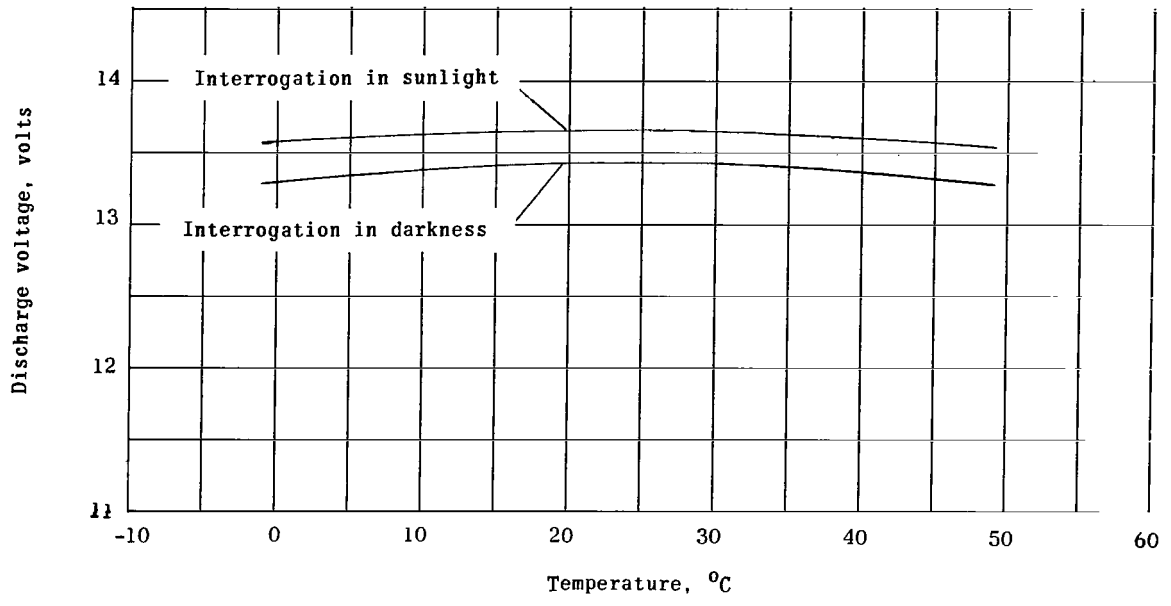

Figure V-13.- Variation of battery discharge voltage with temperature at two orbital conditions.

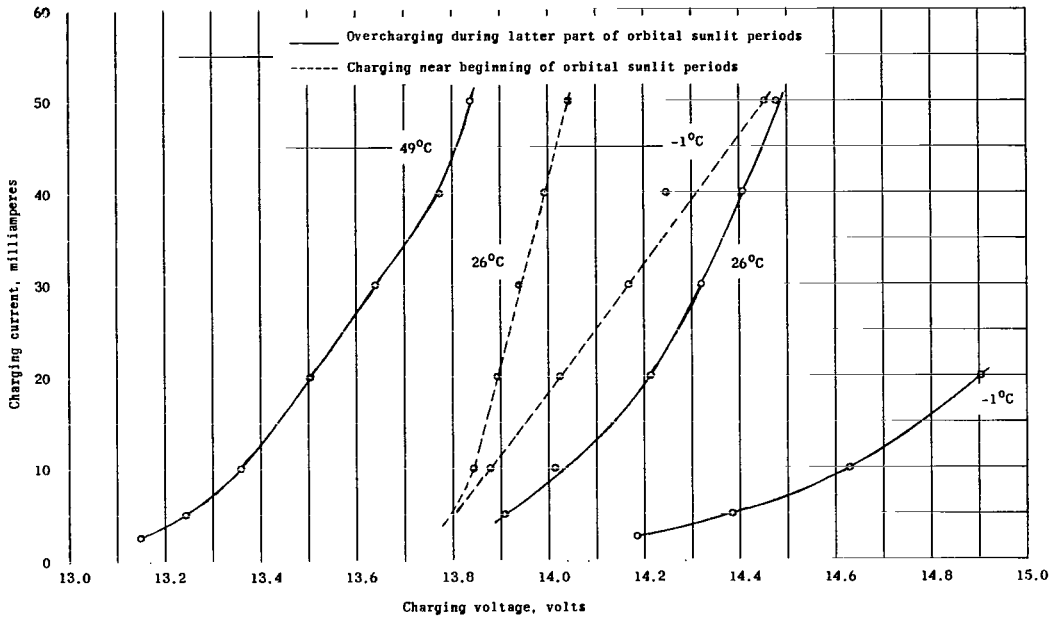

Figure V-14.- Relations between charging voltage, current, and temperature of a typical battery at two simulated orbital conditions.

taken after overcharging for 30 minutes at each current to simulate conditions during the latter part of the orbital sunlit periods. For the dotted curves, the battery was initially fully charged, then discharged at 10 ma for 35 minutes, before charging at the indicated current for 2 minutes. This simulated conditions near the beginning of the orbital sunlit periods. Since high battery temperatures are associated with 100-percent sun, only the overcharging curve is shown for 49° C. It will be noted that at low battery temperatures the charging rate, particularly when overcharging, must be sharply limited to prevent excessively high voltages. At high temperatures, the voltages are inherently low, but overcharging currents must still be limited to prevent excessive internal temperatures and pressures. It was decided that 40 ma was a safe overcharging current at voltages below the allowed maximum.

Another characteristic of these cells that should be mentioned is the possibility of reversed polarity when they are discharged below about 0.9 volt. When a number of cells in series are nearly discharged the lowest capacity cell may reverse while the total voltage is still reasonably high. The discharge current of the other cells will then attempt to charge it in the reverse direction. This results in rapid gas formation, and if a reversal occurs while battery discharge currents are high, a cell may actually explode. To prevent cell reversals, a battery should be made from matched cells thoroughly tested to eliminate defective cells, should not be fully discharged at high rates, and above all, should not be shorted. In the early phases of testing the prototype telemetry, these precautions were not strictly observed, and the damaged battery described in chapter VII was the result.

Qualifying Tests.- Since this button-type battery cell was not designed for space applications, and since the cells received had not been tested by the manufacturer, considerable attention was given to tests designed to detect substandard cells. This testing had to be limited so as not to affect the cell lifetime appreciably. After making a number of inquiries and thoroughly testing sample cells, it was decided to make the following tests on all cells before they were assembled as batteries:

1. Exercising cycle: Starting with the cells completely discharged as received, charge at 40 ma for 16 hours, and then at 30 ma for 4 hours; discharge at 100 ma for 4 hours.

2. Temperature cycles: After recharging the cell to 85 percent of capacity at room temperature, lower cell temperature to -10° C and charge at 10 ma for 1 hour, then discharge at 100 ma for 1 hour, return cells to room temperature and again recharge to 85 percent of capacity. At 49° C, charge at 30 ma for 1 hour, then discharge at 100 ma for 1 hour. At room temperature, discharge at 100 ma for 2 hours.

3. Electrolyte leakage: After cleaning each cell with alcohol, charge at 50 ma for 2 hours, and then at 40 ma for 5 hours. Discharge at 100 ma down to 1.1 volts per cell. Use saturated solution of phenolphthalein to look for evidence of alkalinity.

4. Internal electrical leakage: Charge to 10 percent of capacity and leave for 1 week.

5. Total capacity cycle: Charge at 40 ma for 16 hours, and then at 30 ma for 4 hours; discharge at 100 ma down to 1.1 volts per cell; individually discharge at 30 ma or less down to 1.0 volt.

During these tests, 12 cells were connected in series while in a simple test tray (fig. V-15). Voltage readings were taken periodically, and any abnormal behavior was noted.

In the first order of 120 cells only 15 percent were found to be acceptable. Some of the rejects had defective seals, but the majority of them gradually developed excessive internal resistance, and some became unstable. Internal examination revealed corrosion of the area where the combination loading spring and electrical lead contacted the case.

The supplier then furnished redesigned cells with thin stainless-steel tabs spotwelded to each outer plate and to the appropriate half of the case. About 200 of these improved cells were tested and no defects were found in approximately 75 percent of them.

After the cells were potted in battery modules, they were given another complete charge and discharge cycle. The battery modules for the prototype spacecraft were subjected to the environmental tests described in chapter VII, both individually and while mounted in the telemetry assembly. Subsequent batteries were environmentally tested as part of the telemetry assembly. These tests included simulation of orbital cyclic conditions for several days.

During the several months between battery installation and vehicle launch, they were left unchanged whenever possible, and while charged but not in use they were trickle charged. Approximately 1 week before launching, the batteries were conditioned by a complete discharge and recharge cycle.

SECTION IV - COMPLETE POWER-SUPPLY SYSTEM

Description.- Figure V-16 shows a simplified schematic diagram of each of the two power supplies. The points marked with a cross were available for external measurement of current and voltage during ground testing. Each of the five solar-cell trays was connected through a blocking diode to the nominally 12-volt buss. The type 1N538 blocking diodes were used to prevent the battery discharging through the solar cells when they were not illuminated. Over the current and temperature ranges of interest the forward voltage drop of these diodes varied from 0.68 to 0.78 volt, with 0.75 volt being a typical value. The reverse leakage current per diode was

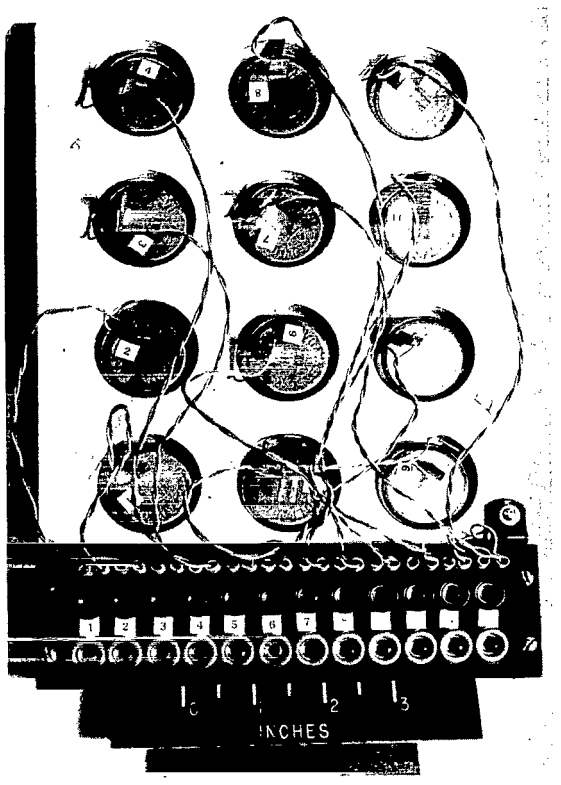

L-60-3179

Figure V-15.- Nickel-cadmium cell test tray.

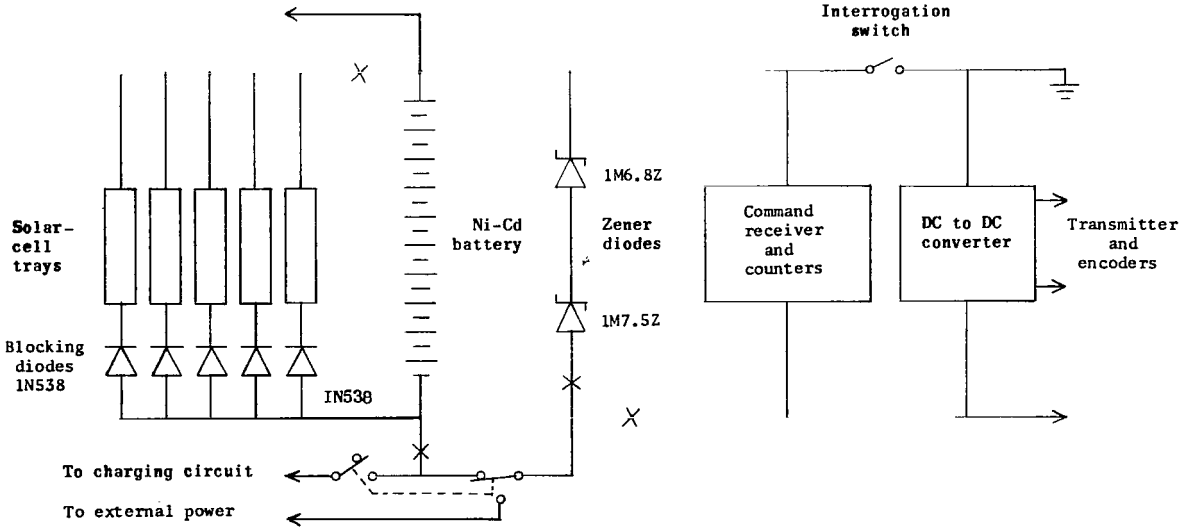

Figure V-16.- Simplified schematic of power supply.

less than 0.2 μa, even at maximum expected temperature. The diode installation is shown in figure V-11.

The zener diodes were used to protect the batteries from excessive charging voltages and currents. It was necessary that zener voltages and battery voltages be well matched over the expected temperature range to insure adequate battery charging as well as protection, and to minimize battery drain by the zeners during orbital darkness. Unfortunately, the effect of temperature on the battery charging voltages (fig. V-14) was opposite to that on the voltage of high-voltage type of zeners, and the temperature coefficient of zeners increased with nominal voltage rating. It was decided to use two 1-watt, 1-percent zeners in series, one having a nominal zener voltage of 6.8 volts and the other 7.5 volts, giving a total nominal value of 14.3 volts. As indicated in figures IV-3 and IV-4, the zeners are installed on top of the telemetry assembly, where they would be at about the same temperature as the batteries. Figure V-17 gives the relations between measured voltage, current, and temperature for a typical pair of zener diodes in series.

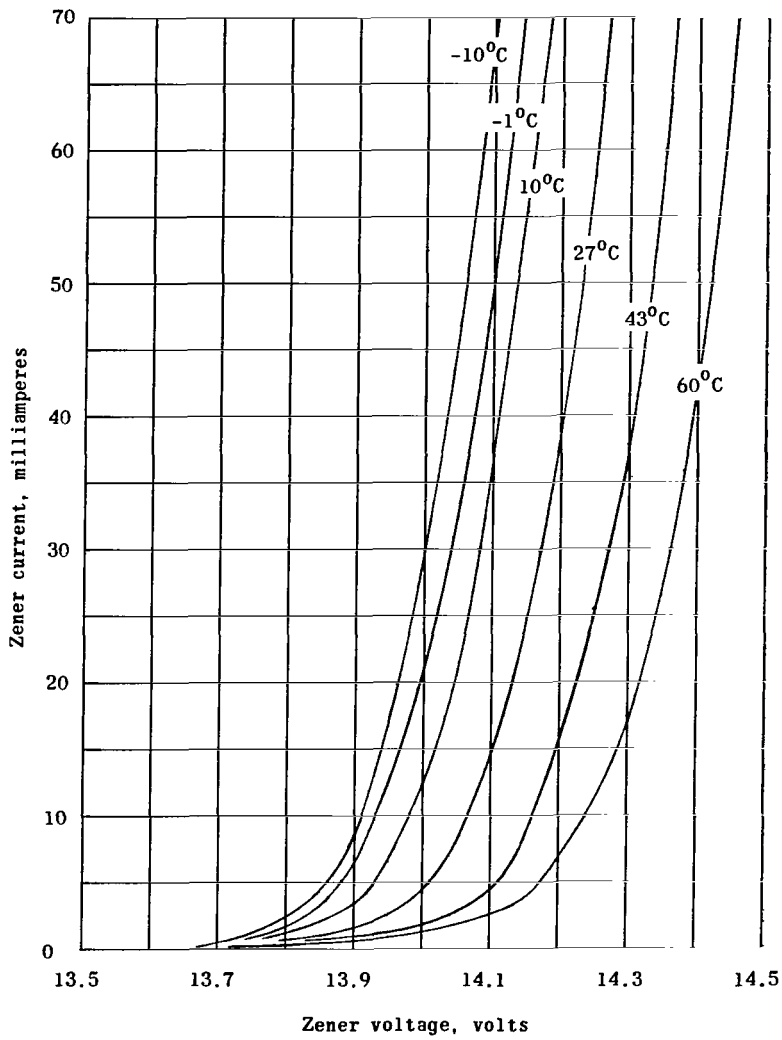

Figure V-17.- Relations between voltage, current, and temperature for a typical pair of zener diodes in series.

System Operation.- Figure V-18 illustrates the graphical method used to help to predict the power-supply buss voltages and the division of currents during various charging conditions in orbit, particularly when considering various zener diode circuits. The solar-cell-output currents shown are those given by the appropriate temperature curve of figure V-4 multiplied by the applicable attitude factor from figure V-8. The other curves were obtained by adding a standby load current of 10 ma to the sum of the battery-charging currents from figure V-14 and the zener currents from figure V-17, at the same voltages and temperatures. The operating points of interest are obviously

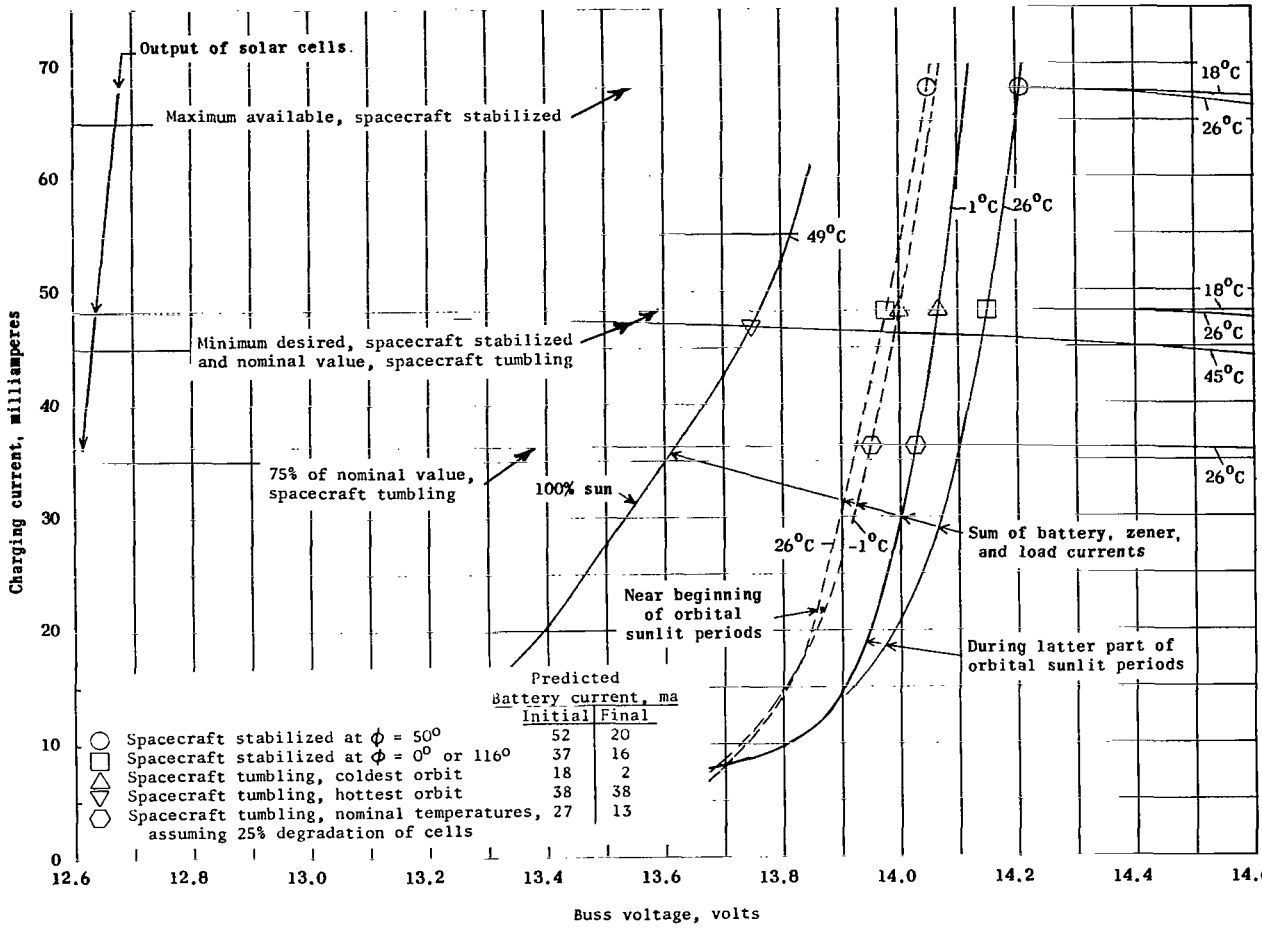

Figure V-18.- Graphical determination of power-supply voltages and currents for several extreme standby conditions in sunlight.

the intersections of the appropriate solar-cell-output curves and total load curves. These intersections determine the buss voltage, and then the battery and zener currents can be obtained from figures V-14 and V-17, respectively. Several extreme conditions are illustrated, and the predicted battery currents are listed in figure V-18. In each case, the maximum permitted charging voltages and currents were not exceeded. However, when the temperatures (and the percent time in sunlight) are near maximum, the zener diodes give very little protection against excessive overcharging currents. This lack of protection required that a launch time be selected that would give either moderate telemetry temperatures while spin stabilized or a stabilized attitude prohibiting maximum solar-cell output. In reference to the discussion of solar cells, it was unlikely that sustained overcharging above 40 ma would occur while the batteries are at elevated temperatures after the onset of tumbling.

It is during the coldest orbits, when time in darkness is maximum and telemeter temperatures are low, that recharging of the batteries is slowest. Fortunately, internal battery leakage is lowest at this time and recharging is

quite efficient. Tests were made to simulate orbital conditions for several days to see if the batteries were bing adequately protected and recharged at various extreme conditions. Figure V-19 shows the recorded history, during the fourteenth cycle at coldest simulated orbital conditions, of battery voltage and current, and zener current, with the simulated solar-cell-output current kept at 40 ma. Various points on the curves agree with those previously found for a well-charged battery. The initial battery charging current was higher than inferred by figure V-18 because interrogations were made at the end of the simulated dark periods. In the cycle tests, when 25-percent degradation of solar-cell-output current (fig. V-18) was simulated, recharging of the batteries was still adequate at intermediate and elevated temperatures, but was marginal under coldest orbital conditions.

SECTION V - SOLAR-CELL TEST GROUPS

In addition to the previously described solar cells used in the power-supply system, five groups of solar cells - each consisting of a 5-cell shingle - were mounted on the forward shell to obtain data on the relative effectiveness of protective covers for the cells and to give an indication of the attitude of the vehicle. Three of these shingles can be seen mounted on the forward shell in figure V-1 (on upper end of the spacecraft in the photograph). One of these was protected with a 1/16-inch-thick quartz window; one had 6-mil-thick glass slides cemented to the cells; the other had bare cells. The latter two shingles were cemented to the same tray. Since the three shingles had the same orientation to the sun, and since their output voltages were telemetered on consecutive frequency channels, their relative degradation in the space environment could be directly determined. Thermistors were used to monitor the temperature of each of the two mounting trays.

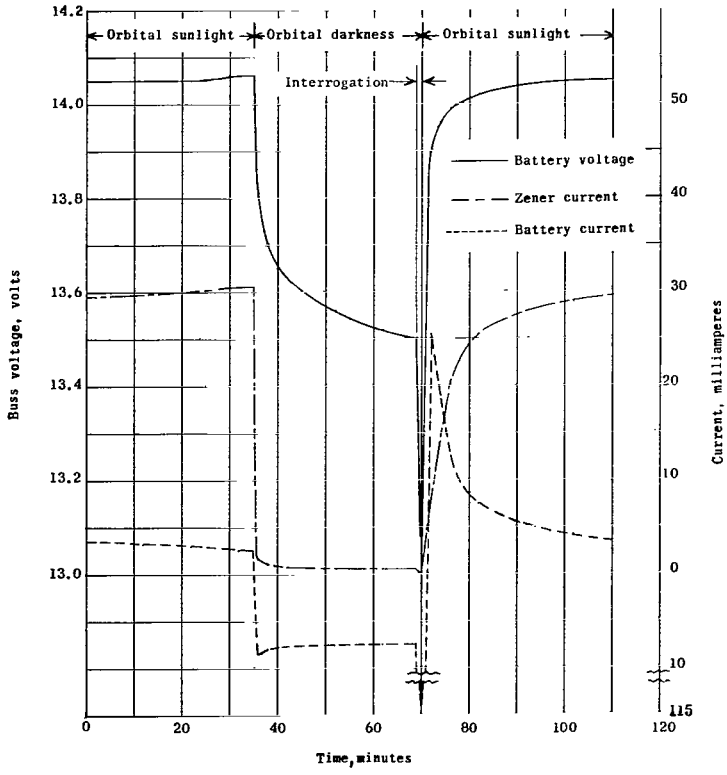

Figure V-19.- History of battery voltage, battery current, and zener current during simulation of coldest orbit.

The other two test groups were mounted 180° apart on the cylindrical side of the forward shell. The one visible in figure V-1 had the 6-mil glass slides cemented to its cells. The other was identical except that its cells were bare. The

telemetered output voltage of these two shingles, together with the data from those on the forward end, was used to estimate the orientation of the vehicle to the sun. With this information, the absolute value of the degradation of each of the five test shingles could be estimated.

Each of the five shingles of test cells consisted of five of the solar cells described previously - ungridded, P on N type, with nominal efficiencies of 8 to 9 percent. Each cell was loaded with 39.2 ohms, which gave an output voltage near the maximum power point of the cells and large enough to drive the voltage-controlled oscillators. The calibration of a typical test shingle against light intensity, at 32° C, is given in figure V-20. Corrections were made for the spectral output of the artificial lights used, and the values of light intensity shown are equivalent to those in space. Figure V-20 also gives the calibration of the same shingle against temperature, at a light intensity of 112 mw/cm^2 (m = 0). The calibrations against angle of incident sunlight varied slightly with the type of cell covering, if any, but in general resembled the solid curve of figure V-6. The test cells were given the same environmental tests as mentioned above for the power trays.

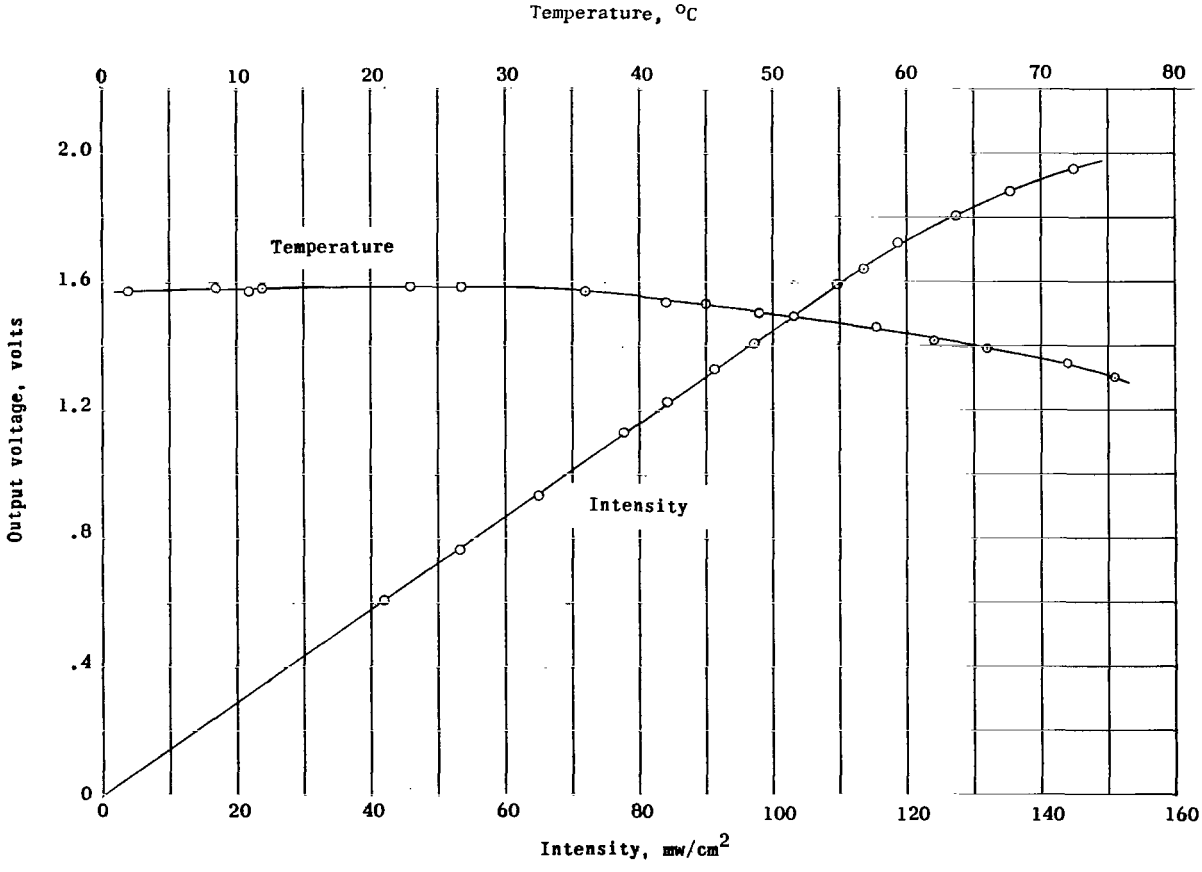

Figure V-20.- Calibration curves of output voltage against light intensity and temperature for a typical test group of solar cells.

SECTION VI - FLIGHT RESULTS

The battery voltages received by telemetry from Explorer XIII were quite close to those predicted by the preflight tests previously described. Although the outputs of the power-supply solar cells were not monitored in flight, the normal battery voltages indicated that both of the power-supply systems survived the launch operations and performed as expected during the life of the spacecraft. No deterioration of the test cells on Explorer XIII was detected. Since interrogations after the fifteenth orbit were made in darkness, the useful exposure time was only about 1 day.

The telemetered output of the test cells indicated that the spacecraft was spin stabilized with its axis approximately 90° from the sun during the interrogated sunlit orbits. Since the telemetry-framing rate was about 3.8 frames/sec compared with the roll rate of about 3.2 rps (obtained from signal strength records), a number of frames had to be examined to get even an approximate attitude. Figure V-21 gives the readings obtained from one group of test cells on the side of the vehicle during the fourteenth orbit. All the readings are plotted relative to the calibrated output obtained for the curve of solar constant against time during a single cycle of roll. Data points from the several telemeter frames during a 14-second period were superimposed to give a composite history of one roll cycle. As indicated, the calibration of output against angle of incident sunlight obtained with the axis of rotation 90° from

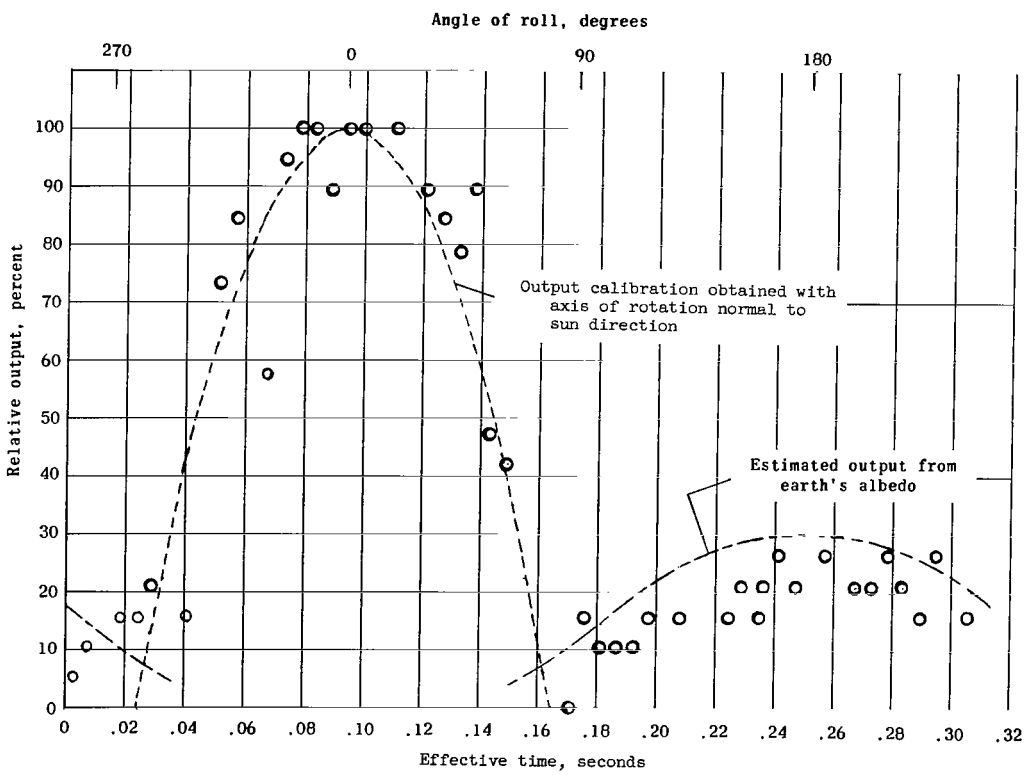

Figure V-21.- Output of test cells on side of vehicle during a portion of the fourteenth orbit.

the sun direction, roughly fitted the higher amplitude readings. The lower amplitude readings approximated the output estimated for the solar cells when rotated away from the sun and illuminated by the earth's albedo.

SECTION VII - APPENDIX A

Ideal Long-Term Average Output of a Solar Cell Randomly Oriented to the Sun

Assume that:

I = Output of solar cell illuminated at normal incidence

I cos ϕ = Output at a light incident angle of ϕ

In spherical coordinates (see fig. V-22(a)),

$$d\beta = \frac{dA}{r^2} = \frac{(r\, d\phi)(r \sin \phi\, d\theta)}{r^2}$$

$$= \sin \phi\, d\phi\, d\theta$$

where β is the solid angle in steradians associated with an area A on the reference sphere of radius r. The output of the solar cell averaged over the 2π steradians above the X-Y plane is

$$\frac{1}{2\pi} \int_0^{2\pi} \int_0^{\pi/2} I \cos \phi\, d\beta$$

$$= \frac{I}{2\pi} \int_0^{2\pi} \int_0^{\pi/2} \cos \phi \sin \phi\, d\phi\, d\theta$$

$$= \frac{1}{2} I$$

Since the solar cell has no output when illuminated from below, its long-term average output when randomly oriented to the sun is 1/4 I.

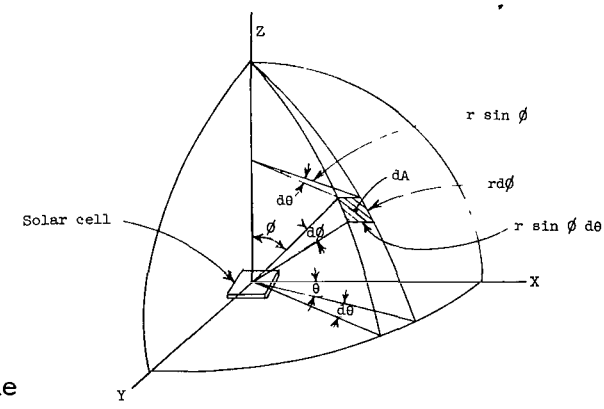

(a) Exact integration in ideal case.

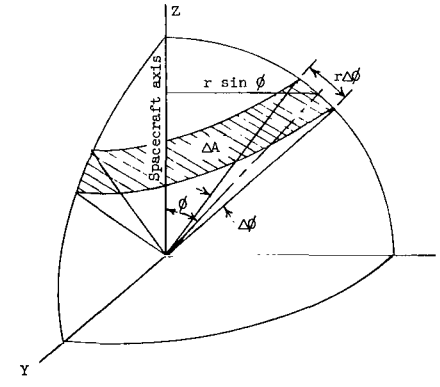

(b) Approximate numerical integration.

Figure V-22.- Spherical axis systems employed in analysis.

SECTION VIII - APPENDIX B

Weighting Factors

To obtain the average output during random tumbling by numerically integrating the curves of figure V-8 (obtained by averaging the output over a spin cycle at various angles of ϕ), each value must be weighted by a factor proportional to the incremental solid angle involved. With reference to figure V-22(b) and the symbol definitions in appendix A, the incremental solid angle is

$$\Delta\beta = \frac{\Delta A}{r^2} = \frac{(r\,\Delta\phi)(2\pi r \sin\phi)}{r^2} = 2\pi\,\Delta\phi \sin\phi$$

If $w_1, w_2, \ldots, w_n$ is a given set of weighting factors, the weighted mean of a given set of output values $I_1, I_2, \ldots, I_n$ is

$$\frac{w_1I_1 + w_2I_2 + \ldots + w_nI_n}{w_1 + w_2 + \ldots + w_n}$$

It will be noted that the constant terms in the weighting factors will cancel, and by using equal values of $\Delta\phi$, the weighting factors of interest are given by $\sin\phi$. The curves of figure V-8 were evaluated at each 10° increment of ϕ. Letting $\Delta\phi = 20^\circ$, the expression for the long-term average output during random tumbling is

$$\frac{I_{10^\circ} \sin 10^\circ + I_{30^\circ} \sin 30^\circ + \ldots + I_{170^\circ} \sin 170^\circ}{\sin 10^\circ + \sin 30^\circ + \ldots + \sin 170^\circ}$$

SECTION IX - REFERENCES

V-1. Hulten, W. C., Honaker, W. C., and Patterson, John L.: Irradiation Effects of 22 and 240 Mev Protons on Several Transistors and Solar Cells. NASA TN D-718, 1961.

V-2. Nash, Harry: Silicon Photovoltaic Cells for Space Vehicles. Electronic Inst., Aug. 1959, pp. 91-106.

V-3. Zoutendyk, John A.: A Method for Predicting the Efficiency of Solar Cell Power Systems Outside the Earth's Atmosphere. Tech. Rep. No. 32-259 (Contract NAS 7-100), Jet Propulsion Lab., C.I.T., Apr. 10, 1962.